Flavor independence and the dual superconducting model of QCD

Lewis P. Fulcher
Physics and Astronomy, Bowling Green State University
Bowling Green, Ohio 43403
email: fulcher@newton.bgsu.edu
(February 1, 2008)

Baker, Ball and Zachariasen have developed an elegant formulation of the dual superconducting model of quantum chromodynamics (QCD), which allows one to use the field equations to eliminate the gluon and Higgs degrees of freedom and thus to express the interaction between quarks as an effective potential. Carrying out an expansion in inverse powers of the constituent quark masses, these authors succeeded in identifying the central part, the spin-dependent part and the leading relativistic corrections to the central potential. The potential offers a good account of the energies and splittings of charmonium and the upsilon system. Since all of the flavor dependence of the interaction is presumed to enter through the constituent masses, it is possible to test the potential in other systems. Logical candidates are the heavy B-flavor charmed system and the heavy-light systems, which should be more sensitive to the relativistic corrections. Lattice gauge calculations furnish an additional point of contact for the components of the BBZ potential. Some preliminary calculations of the energies of B and D mesons are presented and the challenge of agreement with experiment is discussed. The spinless Salpeter equation is used to account for the effects of relativistic kinematics.

12.39.Ki,12.39.Pn,12.38.Aw,12.40.Yx

INTRODUCTION

After an extensive investigation Baker, Ball and Zachariasen [1,2] (BBZ) have developed a number of arguments to support the use of the dual color fields (derived from the color electric vector potential C_μ), instead of the usual Yang-Mills fields (derived from the magnetic vector potential A_μ), to formulate an effective theory of long-distance quantum chromodynamics (QCD). The Dyson-Schwinger equation may be used to justify some of their arguments, since it shows that corrections to the leading terms in the A_μ propagator Δ_A are more singular in the infrared region that the leading term. This behavior is not true for the C_μ propagator, and thus one should use the dual fields in the long-distance region. Furthermore, BBZ argue that the connections between the dual fields and the Yang-Mills fields are nonlocal and require the introduction of an additional field. They use this requirement to good advantage by introducing Higgs fields, which allow a symmetry breaking mechanism to operate and thus confinement is explained as a Meissner effect, in the spirit of the 't Hooft-Mandelstam conjecture [3,4], where a magnetic condensate exerts pressure on the gluon field lines. The BBZ Lagrangian leads to an effective field theory with many of the properties expected from QCD, such as unitarity, renormalizability and non-Abelian gauge invariance. One can also show that the theory undergoes a deconfinement transition [5]. A recent examination of the foundations of the BBZ model [6] led to a reformulation of the theoretical underpinnings in a Wilson loop context.

In their more recent work BBZ [7–9] have constructed an interaction potential between a quark source and its antiquark by developing an expansion in inverse powers of the constituent masses. They use the field equations to eliminate the gluon and the Higgs fields and express the interaction energy in terms of the quark and antiquark variables. They can readily identify the central potential, the spin-dependent potentials and the leading relativistic corrections to the central potential. In this paper we explore some of the problems that arise when one attempts to use this potential in systems where relativistic corrections are more important. In particular, we attempt to give a simultaneous account of the properties of charmonium, the upsilon system and the heavy light systems using the spinless Salpeter equation [10] for relativistic kinematics and a single set of potential parameters [11,12]. In addressing this issue we will be led to examine questions about the relationships between the constants in the BBZ potential components and the parameters associated with mass renormalization [13]. We note in passing the interesting work of Crater and Alstine [14,15] that explores the question of a universal quark-antiquark potential in the context of the Todorov equation and constraint dynamics.

Since spin dependence is not a natural companion to work based on the spinless Salpeter equation, we will focus on spin-averaged energies as the point of contact with experiment. This goal is consistent with the goal of the BBZ investigations to produce an effective theory of long-range QCD, since spin-dependent splittings are presumably more sensitive to the short-range behavior of the potentials, where running coupling constant effects are important.

Although it is possible to accomodate such effects within the framework of the BBZ model, this involves additional assumptions [16]. We have plans to pursue the role of the spin dependence in the context of the work of Hardekopf and Sucher [17].

Our method of solution of the spinless Salpeter equation is based on a recent improvement [18,19] of the Rayleigh-Ritz-Galerkin method. The purpose of our calculation is to see how successful one can be with the leading relativistic corrections and what role experiments might play in constraining these corrections and their relativistic generalizations. We establish contact with recent precision lattice gauge calculations of Bali, Schilling and Wachter [20,21] in order to have an additional guide for evaluating the relativistic corrections.

The highpoints of the BBZ formalism are summarized in Sec. I, and the solution of the spinless Salpeter equation is presented in Sec. II. Some of the problems associated with the Salpeter wave functions and the salient features of the interpretation of the momentum operators are discussed in Sec. III. Our results and conclusions are presented in Sec. IV.

I. BBZ MODEL

The fundamental degrees of freedom of the BBZ model are an octet of dual gluon potentials $C_\mu^a\,(a=1,\ldots,8)$ and a triple of scalar Higgs fields $\vec{B}^a$. Because of the symmetry breaking mechanism, these Higgs fields have nonzero vacuum expectation values, which give rise to effective masses for the dual gluons and two of the scalar Higgs fields. These effective masses are responsible for the exponential damping of all fields outside of the region of the sources and the flux tube that connects them. The model is based on the Lagrangian density,

$$\mathcal{L} = TR\left[\left(\mathbf{H}^2-\mathbf{D}^2\right)+\left(D_\mu\vec{B}\right)^2\right]-W(\vec{B}), \tag{1}$$

where all the field variables in Eq. (1) are scalar products with the SU(3) color matrices λ_a (e.g. $C_\mu \equiv \frac{1}{2}\,\Sigma\, C_\mu^a\lambda_a$) and $W(\vec{B})$ denotes the Higgs potential. The covariant derivative in Eq. (1),

$$D_\mu\vec{B} \equiv \partial_\mu\vec{B} - ig\left[C_\mu,\vec{B}\right], \tag{2}$$

is necessary for non-Abelian gauge invariance. The electric displacement $\mathbf{D}$ and the magnetic field $\mathbf{H}$ are related to the vector potential C_μ by the non-Abelian relations,

$$\mathbf{D} = -\nabla\times\mathbf{C} - \frac{\mathrm{ig}}{2}\left[\mathbf{C},\times\mathbf{C}\right], \tag{3a}$$

$$\mathbf{H} = -\nabla C_0 - \partial_0\mathbf{C} - ig\left[\mathbf{C},C_0\right]. \tag{3b}$$

To derive the simplest set of field equations with non-Abelian couplings, BBZ choose a gauge where the components of the Higgs triple point in three independent color directions, namely, $\vec{B}=(\lambda_7 B_1,-\lambda_5 B_2,\lambda_2 B_3)$ and all the dual gluon field variables are proportional to the color matrix $Y=\lambda_8/\sqrt{3}$. This particular choice leads [22] to finite results for the commutators of the first two components of $\vec{B}$ in Eq. (2), but the remaining commutators in the equations above vanish. Thus all the relationships in the gluon sector are Abelian. Evaluating the trace of Eq. (1) yields

$$\mathcal{L} = \frac{2}{3}\left(\mathbf{H}^2-\mathbf{D}^2\right)+2\,\partial_\mu\vec{B}\cdot\partial^\mu\vec{B}+2\,g^2C_\mu C^\mu\left(B_1^2+B_2^2\right)+W(\vec{B}). \tag{4}$$

Since this Lagrangian density is symmetric in the components B_1 and B_2, we may choose them to be equal. The fourth-order term in Eq. (4) leads to effective mass terms in the field equations of the dual vector potential C_μ and the first two components of $\vec{B}$, thus restricting these fields to the flux tube region and its vicinity.

To complete the calculation of the interaction energy of a quark and its antiquark, one must introduce these particles as classical sources with masses m_1 and m_2 and spins σ_1 and σ_2, which are located at $\mathbf{x}_1$ and $\mathbf{x}_2$ and connected by a Dirac string. It is important to isolate the string contributions to the electric displacement and the magnetic field, $\mathbf{D}_\mathrm{S}$ and $\mathbf{H}_\mathrm{S}$, which are produced by the sources,

$$\rho(\mathbf{x}) = e\left[\delta^3(\mathbf{x}-\mathbf{x}_1)-\delta^3(\mathbf{x}-\mathbf{x}_2)\right]Y, \tag{5a}$$

$$\mathbf{j}(\mathbf{x}) = e\left[\mathbf{v}_1\delta^3(\mathbf{x}-\mathbf{x}_1) - \mathbf{v}_2\delta^3(\mathbf{x}-\mathbf{x}_2)\right]Y, \tag{5b}$$

where the velocities $\mathbf{v}_{\rm i}$ are simply the time derivatives of the quark coordinates $\mathbf{x}_{\rm i}$. The relationships between the fields and the potentials also include explicit contributions from the color magnetization $\mathbf{M}$ and the color polarization $\mathbf{M}$, which arise from the spin dependence of the sources. Thus,

$$\mathbf{D} = -\nabla\times\mathbf{C} + \mathbf{D}_{\rm S} - \mathbf{P}, \tag{6a}$$

$$\mathbf{H} = -\nabla{\rm C}_0 - \partial_0\mathbf{C} + \mathbf{H}_{\rm S} + \mathbf{M}. \tag{6b}$$

From the Lagrangian density of Eq. (4) one can derive the field equations for the vector potential C_μ and the Higgs fields $\vec{B}$. Their couplings to the sources are given by Eqs. (6), and thus the energy content of the fields surrounding the sources is completely determined by the solution to these field equations. Substituting these solutions into the expression for the Lagrangian density and integrating over all space gives the energy of the quark-antiquark system as a function of the source parameters $\mathbf{r} = \mathbf{x}_1 - \mathbf{x}_2$, $\mathbf{v}_{\rm i}$ and $\sigma_{\rm i}$. Thus the potential is given by

$$V(\mathbf{r},\mathbf{v}_{\rm i},\sigma_{\rm i}) = -\int d^3x\,\mathcal{L}(\mathbf{x},\mathbf{v}_{\rm i},\sigma_{\rm i},\mathbf{C},\partial_{\rm j}\mathbf{C},\vec{\rm B}). \tag{7}$$

It is straightforward to identify the central potential, the spin-dependent potential and the velocity-dependent corrections to the central potential, that is,

$$V = V_0 + V_{SD} + V_{v^2}, \tag{8}$$

where the central potential is given by

$$V_0 = Ar - \frac{4\alpha_S}{3r}e^{-0.511\sqrt{A/\alpha_S}\,r} - 0.646\sqrt{A\alpha_S}. \tag{9}$$

It is not necessary to list the spin-dependent potential here, since it will not contribute to the spin-averaged energies in the lowest order. The velocity-dependent corrections to the central potential are given by the sum of an angular-momentum term and a radial-momentum term, namely, $V_{v^2} = V_{ang} + V_{rad}$. Each of these terms consists of two parts,

$$V_{ang} = V_+\ \left[\mathbf{r}\times(\mathbf{v}_1-\mathbf{v}_2)\right]^2/4{\rm r}^2\ +\ {\rm V}_-\ \left[\mathbf{r}\times(\mathbf{v}_1+\mathbf{v}_2)\right]^2/4{\rm r}^2, \tag{10a}$$

$$V_{rad} = V_\parallel\ \left[\mathbf{r}\cdot(\mathbf{v}_1+\mathbf{v}_2)\right]^2/4{\rm r}^2\ +\ {\rm V_L}\ \left[\mathbf{r}\cdot(\mathbf{v}_1-\mathbf{v}_2)\right]^2/4{\rm r}^2. \tag{10b}$$

The potentials listed in Eqs. (10) are not all independent. Because of the Lorentz covariance of the theory [9,13], two of them may be expressed in terms of the central potential as follows:

$$V_- = -\frac{1}{2}V_0 \qquad ; \qquad V_\parallel = V_- + \frac{r}{2}\frac{\partial V_0}{\partial r}, \tag{11}$$

BBZ [9] list explicit results for the other two,

$$V_+ = -\frac{2\alpha_S}{3r}e^{-1.14\sqrt{A/\alpha_S}\,r} - 0.208Ar + 1.12\sqrt{A\alpha_S}, \tag{12a}$$

$$V_L = -\frac{4\alpha_S}{3r}e^{-0.685\sqrt{A/\alpha_S}\,r} + 0.0885\sqrt{A\alpha_S}. \tag{12b}$$

Thus only two parameters, the string constant A and the strong coupling constant α_S are required to determine the potential. Of course, in the center-of-momentum frame the constituent masses become part of the parametrization through the relations, $\mathbf{v}_1 = \mathbf{p}/{\rm m}_1$ and $\mathbf{v}_2 = \mathbf{p}/{\rm m}_2$. Since agreement with experiment will not be easy to achieve, it is important to explore the sensitivity of the calculation to various parts of V_{v^2}. Thus we report results below where the form of the longitudinal component is changed to

$$V_L' = -\frac{4\alpha_S}{3r}. \tag{13}$$

and to

$$V_L'' = -\frac{4\alpha_S}{3r} e^{-0.685\sqrt{A/\alpha_S}\, r}. \tag{14}$$

In the limit of perturbative QCD ($A \to 0$) the potentials V_+, V_-, $V_\parallel$, V_L all reduce to multiples of the Coulomb potential. Thus, the central potential and its leading relativistic correction reduce to the Darwin limit [23],

$$V_0 + V_{v^2} \to -\frac{4\alpha_S}{3r}\left[1 - \frac{1}{2}\ (\mathbf{v}_1 \cdot \mathbf{v}_2 + \mathbf{v}_1 \cdot \hat{\mathbf{r}}\ \mathbf{v}_2 \cdot \hat{\mathbf{r}})\right]. \tag{15}$$

We determine our parameters in the heavy quark systems, where the expansion in powers of the inverse masses is expected to have the most validity. Using the spin-averaged 1S, 2S and 1P energies of the upsilon system [24] and the 1S energy of charmonium, we find that

$$A = 0.235\, GeV^2;\ \frac{4}{3}\alpha_S = 0.398;\ m_b = 4.710\, GeV;\ m_c = 1.320\, GeV, \tag{16}$$

for the case that V_L is given by Eq. (13) above.

II. SOLUTION OF THE SPINLESS SALPETER EQUATION

Our semirelativistic potential model is based on the Salpeter equation, $H\Psi_n = E_n\Psi_n$, where

$$H = \sqrt{m_1^2 + p^2}\ + \sqrt{m_2^2 + p^2}\ + V(\mathbf{r}, \mathbf{p}), \tag{17}$$

and the potential is given to $O(v^2)$ by Eq. (8). This model may be thought of as a three-dimensional reduction of the Bethe-Salpeter equation [10,25]. We will find the exact solution to this equation with the central potential of Eq. (9) using the approach of Refs. [18,19] to the Rayleigh-Ritz-Galerkin method, where the wave function Ψ_n is expanded in terms of a complete set of basis functions. Then we will add the effects of V_{v^2} with a first-order perturbation improvement.

The basis functions [10,18,19,26] used for the calculation include a spherical harmonic factor $Y_{\ell m}(\hat{\mathbf{r}})$ and the radial functions,

$$R_{n\ell} = N_{n\ell}\beta^{3/2}(2\beta r)^\ell e^{-\beta r} L_n^{2\ell+2}(2\beta r), \tag{18}$$

where $N_{n\ell}^2 = 8(n!)/\Gamma(n + 2\ell + 2)$, β is a scale parameter, and the oscillations necessary for completeness are supplied by the associated Laguerre polynomials $L_n^{2\ell+2}(2\beta r)$. Two important advantages accompany the use of these basis functions. The first of these is that all of the basic matrix elements that we require to find the eigenvalues and the eigenfunctions of Eq. (17) can be generated from straightforward analytic expressions. The second is that the confinement factors of Eq. (18) are a sufficiently good approximation to the actual wave function that the sizes of the requisite matrices are relatively modest (20×20 or 40×40). Analytic expressions for the matrix elements of the operators $(p^2)_{nn'}$, the linear potential, $(Ar)_{nn'}$, and the Coulomb potential $(-4\alpha_S/3r)_{nn'}$ are listed in Ref. [19]. There it is also explained how one can calculate the matrix elements of the nonlocal kinetic energy operators in Eq. (17) by effectively taking the square roots of the matrix representations of the operators $m_i^2 + p^2$.

Thus the remaining challenge in finding the solutions to the Hamiltonian operator of Eq. (17) resides in the Yukawa factor present in the central potential of Eq. (9). We write the central potential as a Cornell Potential (linear + Coulomb) and a residual part by adding and subtracting a Coulomb piece, that is,

$$V_0 = V_{Cornell} + \frac{4\alpha_S}{3r}\left(1 - e^{-\eta r}\right), \tag{19}$$

where $\eta = 0.511\sqrt{A/\alpha_S}$. To determine the matrix elements of the residual part, we use the following algorithm:

1. Generate the matrix elements of the r_{op}, that is, the $(r)_{nn'}$.
2. Diagonalize this matrix to find the eigenvalues r_k, which give a unique signature of r_{op} in the chosen Hilbert space.

3. From the diagonal elements form the quantities $f(r_k) = (1 - e^{-\eta r_k})/r_k$, which constitute a signature of the residual part of the potential of Eq. (19).

4. Restore to the original basis with the unitary transformation that connects the original matrix representative of r_{op} to its diagonal signature.

5. Examine the procedure for stability by varying the sizes of the matrices.

In order to have a definitive test for the stability of this five-step algorithm, it is convenient to have analytic results for some of the low-lying S-state matrix elements. With the basis functions of Eq. (18) it is straightforward to evaluate a few matrix elements of the residual operator $f(r)$ when $\ell = 0$. We list five of these from the first two rows of the matrix,

$$(f)_{00} = \frac{\beta\delta(2+\delta)}{(1+\delta)^2}\ ;\ (f)_{01} = \frac{\beta\delta^2(3+\delta)}{\sqrt{3}(1+\delta)^3}, \tag{20a}$$

$$(f)_{02} = \frac{\beta\delta^3(4+\delta)}{\sqrt{6}(1+\delta)^4}, \tag{20b}$$

$$(f)_{11} = \frac{\beta\delta(2+3\delta+4\delta^2+\delta^3)}{(1+\delta)^4}, \tag{20c}$$

$$(f)_{12} = \frac{\beta\delta^2(4+4\delta+5\delta^2+\delta^3)}{\sqrt{2}(1+\delta)^5}, \tag{20d}$$

where $\delta = \eta/(2\beta)$. We have verified that the matrix elements of Eq. (20) have the correct small η behavior, where a power series expansion is valid, and the correct large η behavior, where the matrix elements must reduce to those of the Coulomb potential.

The results for the stability study of the matrix elements of the function $f(r)$ are presented in Table I. There results are listed for five different matrix sizes used to find the eigenvalues of r_{op}, as discussed in step 2 of the algorithm below Eq. (19). Since there is no discernible difference in the matrix elements listed in the middle four columns and these results agree with the analytic results, one concludes that using a 40×40 matrix should generate very accurate results for $(f)_{nn'}$. The energy eigenvalues listed in Table I were obtained with kinetic energy matrices the same size as the potential energy matrices. For the three smaller cases the Hamiltonian matrices were also chosen the same size as the kinetic and potential energy matrices, but for the two larger cases a 20×20 matrix was used for the Hamiltonian matrix. All of these results are consistent with our earlier study [19] of the stability of the algorithm used to take the square roots of the kinetic energy operator and the choice of 20×20 as adequate for the Hamiltonian matrix.

In summary our calculation of the energy eigenvalues and eigenfunctions requires four separate matrix diagonalizations, two to determine the kinetic energy operators, one to determine the residual operator $f(r)$, which represents the difference between the Yukawa potential and the Coulomb potential, and a fourth to diagonalize the Hamiltonian matrix. For the first three diagonalizations we use 40×40 matrices, and for the last we use a 20×20 matrix. One can generate accurate results for a range of scale values. The choice $\beta = 2.0\,\mathrm{GeV}$ is a good one for the upsilon system, but $\beta = 1.0\,\mathrm{GeV}$ is better for the heavy-light systems.

III. VELOCITY-DEPENDENT CORRECTIONS

Working in the center-of-momentum frame, where $\mathbf{v}_1 = \mathbf{p}/\mathrm{m}_1$ and $\mathbf{v}_2 = -\mathbf{p}/\mathrm{m}_2$, allows us to write the velocity-dependent potentials of Eq. (10) in the form,

$$V_{ang} = \left[\left(\frac{1}{m_1} + \frac{1}{m_2}\right)^2 \frac{V_+}{4r^2} + \left(\frac{1}{m_1} - \frac{1}{m_2}\right)^2 \frac{V_-}{4r^2}\right](\mathbf{r}\times\mathbf{p})\cdot(\mathbf{r}\times\mathbf{p}), \tag{21a}$$

$$V_{rad} = \left[\left(\frac{1}{m_1} - \frac{1}{m_2}\right)^2 \frac{V_\parallel}{4r^2} + \left(\frac{1}{m_1} + \frac{1}{m_2}\right)^2 \frac{V_L}{4r^2}\right](\mathbf{r}\cdot\mathbf{p})(\mathbf{r}\cdot\mathbf{p}). \tag{21b}$$

It is important to note that Eq. (21) is a classical expression for the velocity-dependent potential energy of two classical sources, and thus it carries no instructions for ordering the momentum and position operators. Certainly, the quantum mechanical generalization of Eq. (21) must respect the principle of Hermiticity. Although this principle is an adequate guide to determine the appropriate combination of any two noncommuting operators, some additional considerations are required for more complicated combinations. To resolve the ambiguity, we choose to interprete the combinations of momentum and position operators in Eq. (21) with the Gromes [27] double-bracket notation,

$$\{\{p_i F(\mathbf{r}) p_j\}\} = \frac{1}{4}\left[p_i F p_j + p_j F p_i + p_i p_j F + F p_i p_j\right]. \tag{22}$$

This expression has the virtue that it is manifestly Hermitian and that it is involved in the nonrelativistic reductions of several covariant Dirac potentials.

One additional difficulty requires some comment. The S-state expectation value of V_{v^2}, the first-order perturbation theory improvement, leads to singular integrals. Such terms arise because of the dominant influence of the Coulomb part of V_0 upon the Salpeter wave function at short distances. Nickisch, Durand and Durand [28] have shown that the small r behavior of the 1S radial function is given by $R_{1S}(r) \to Br^{-\rho}$, where $\rho \approx 0.25$ for realistic values of α_S. To illustrate this behavior we choose one of the factors that arises from the last term of V_{rad}, that is

$$I_L = \int_0^\infty dr\, r^2 \left(\frac{\partial R_{n\ell}}{\partial r}\right)^2 V_L. \tag{23}$$

The small r behavior of the integrand is given by $G(r) \to -4\alpha_S B^2\rho^2/3r^{1+2\rho}$, which leads to a divergent integral at the lower limit. An important part of the reason for this divergence can be traced to the nonrelativistic limit used for the velocity operators. The relativistic expressions for the velocity operators of Eq. (10) are $v_i = p/\sqrt{m_i^2+p^2}$, which have a finite large-momentum limit, in contrast to $v_i \approx p/m_i$, which we used to obtain Eq. (21). Thus, the constituent masses should provide a high-momentum cutoff in a more accurate treatment. Translating this observation into position space suggests that the Compton wavelengths of the constituent quarks should provide a short-distance cutoff, which would prevent the singular behavior. Since the singular behavior arises in the perturbative limit of Eq. (15) and this equation is symmetric in the two masses, we choose a cutoff that is the geometric mean of the constituent Compton wavelengths, that is, $\Lambda = (m_1 m_2)^{1/2}$. This choice does not introduce any new paramters into the calculation. Since all of the singular integrals that arise in the calculation of the expectation value of V_{v^2} have exactly the same behavior, one cutoff suffices to eliminate this behavior.

IV. RESULTS AND DISCUSSION

Our results for the 1S B meson masses are shown in Fig. 1, where they are compared with the spin averages of the measured B meson masses [29]. The full Salpeter curve shows the results of a calculation with the central potential of Eq. (9) only. This curve exhibits a uniform decrease, as the light quark masses decreases, in contrast to the pathological behavior [25,30] of the Schrödinger equation results. It suggests that the Salpeter equation is a reasonable starting point for a potential model calculation since it is not too far above the data. The remaining four curves of Fig. 1 include the effects of the velocity-dependent potential V_{v^2} of Eq. (10). Each of these curves include perturbative and nonperturbative effects since they use the same expressions for V_+, V_- and $V_\parallel$. The dotted curve is based on the last of Eqs. (12) for V_L. Thus it includes all of the physics described by the BBZ model. In contrast, the dashed curve includes only perturbative effects in V_L, since it is based on Eq. (13). The relativistic correction of the dotted curve has the wrong sign to move the Salpeter results towards agreement with experiment. The appearance of a pronounced minimum near 0.325 GeV shows the return of nonphysical behavior similar to the Schrödinger results, that is, the mass of the system increases as the constituent mass decreases. Such behavior has also been noted by BBZ in an Appendix of Ref. [9]. However, the results of the dashed curve exhibit the characteristics necessary for agreement with experiment. The dashed curve intersects the measured values near $m_u = 0.180\,\mathrm{GeV}$ and $m_s = 0.220\,\mathrm{GeV}$, which are reasonable values for the constituent masses [16,31,32].

The remaining two curves in Fig. 1 are based on additional modifications of V_L or V_{v^2}, which might be helpful in isolating the reasons behind the striking differences between the dotted and dashed curves there. The dot-short dashed curve of Fig. 1 is based on Eq. (14). All of the difference between this curve and the dashed curve is due to the exponential damping of the Yukawa factor. Such a pronounced dependence is a consequence of the r^2 weighting of the integrand of the cutoff form of the integral of Eq. (23).

The long and short dashed curve is the result of an attempt to see if the freedom implicit in mass renormalization can be helpful in removing the discrepancy between the BBZ model (dotted curve) and experiment. Barchielli,

Brambilla and Prosperi [13] show that a redefinition of the constituent masses leads to changes in the components of the velocity-dependent potential V_{v^2}—at least in the nonrelativistic limit—, since, if one makes the replacement $m_i \to m_i + \Delta$, the Hamiltonian

$$H = m_1 + m_2 + \frac{p^2}{2m_1} + \frac{p^2}{2m_2} + V_0 + V_{SD} + V_{v^2}, \tag{24}$$

is changed to

$$H_R = m_1 + m_2 + 2\Delta + \frac{p^2}{2m_1} + \frac{p^2}{2m_2} - \frac{\Delta}{2}\left(\frac{p^2}{m_1^2} + \frac{p^2}{m_2^2}\right) + V_0 + V_{SD} + V_{v^2}. \tag{25}$$

The two Δ-dependent terms can be absorbed in a redefinition of the potentials V_0 and V_{v^2}. However, one must be careful to respect the momentum dependence prescribed by the form of Eq. (25). This requires that the same constant be subtracted from each of the component potentials, V_+, V_-, $V_\parallel$ and V_L. The potential parameters obtained by requiring the "mass–renormalized " component potentials to fit the upsilon energy differences are identical to those obtained with the full BBZ potentials, as expected. The differences between the long and short dashed curve and the dotted curve, which become larger at smaller values of the light quark mass, probably reflect the fact that one requires a different mass renormalization procedure in this region.

It is worth noting that the parameters used to obtain each of the curves in Fig. 1 are slightly different, since in each case they were obtained by fitting the energy levels of the heavy quark systems. For example the dotted curve is based on the set, $A = 0.229\,\mathrm{GeV}^2$, $\alpha_S = 0.307$, $m_b = 4.717\,\mathrm{GeV}$and $m_c = 1.308\,\mathrm{GeV}$, which differ slightly from the values listed in Eq. (16), the set used to calculate the dashed curve. The potential parameters for the two remaining curves in Fig. 1 are identical to those for the dotted curve.

The results for the 1S D meson masses depicted in Fig. 2 are very similar to those of Fig. 1, since each curve there has the same qualitative features as its counterpart in Fig. 1. The dashed curve in Fig. 2 intersects the measured masses near $m_u = 0.130\,GeV$ and $m_s = 0.200\,GeV$. These values differ somewhat form those determined in Fig. 1, but such differences could easily be accounted for by a running mass.

Results for the P state masses of the D mesons are presented in Fig. 3. The dotted curve has a shallow minimum around 0.275 GeV, in qualitative accord with the S state behavior. The dashed curve again intersects the data points, but the values that one obtains for the constituent masses, namely $m_u = 0.110\ GeV$ and $m_s = 0.125\ GeV$ are uncomfortably close together. The remaining two dashed curves in Fig. 3 have qualitative differences from their S state counterparts.

Thus, our conclusion is that we have not been able to use the full BBZ potentials to simultaneously account for the energies of the heavy quark systems and the heavy flavour systems with a single set of potential parameters in the context of the spinless Salpeter equation. It will be very interesting to see if calculations based upon the formalism of Hardekopf and Sucher [17] will remove this discrepancy.

Since lattice gauge calculations are becoming more and more accurate, it is worthwhile to examine the recent calculations [21] of Bali, Schilling and Wachter (BSW) to see if they contain any guidance about which form of V_L is best to use. BSW present results for the velocity-dependent spin-independent corrections V_b, V_c, V_d, V_e, which are defined as in the recent work of Brambilla and Vairo [33]. These component potentials are certain linear combinations of the potentials V_+, V_-, $V_\parallel$, V_L. For example, V_c and V_e are defined by the relations,

$$V_c = \left(V_- + V_L - V_+ - V_\parallel\right)/2, \tag{26a}$$

$$V_e = \left(V_+ + V_- - V_\parallel - V_L\right)/4. \tag{26b}$$

In Fig. 4 we compare two of our determinations of V_c with representative lattice data taken from Fig. 15 of Ref. [21]. The dotted curve there is based on the use of Eq. (12) for V_L and the paramter set listed above in this section. The dashed curve there is based on the use of Eq. (13) for V_L and the parameter set of Eq. (16). The lattice data does seem to favor the dotted curve over the dashed curve, but the error bars in the lattice data are large enough to prevent any strong indication. It is worth noting how much more sensitive the energy level calculations are to the differences between these two cases than the potential of Fig. 4.

---

[1] M. Baker, J. Ball and F. Zachariasen, Phys. Rev. D **37**, 1036 (1988).

[2] M. Baker, J. Ball and F. Zachariasen, Phys. Rep. **209**, 73 (1991).
[3] G. 't Hooft, in *Proceedings of the European Physical Society Conference on High Energy Physics*, 1975, edited by A. Zichichi (Editrice, Compostori, Bologna, 1976).
[4] S. Mandelstam, Phys. Rep. **23C**, 245 (1976)
[5] M. Baker, J. Ball and F. Zachariasen, Phys. Rev. Lett. **61**, 521 (1988).
[6] M. Baker, J. Ball, N. Brambilla, G. Prosperi and F. Zachariasen, Phys. Rev. D **54**, 2829 (1996).
[7] M. Baker, J. Ball and F. Zachariasen, Phys. Rev. D **44**, 3328 (1991).
[8] M. Baker, J. Ball and F. Zachariasen, Phys. Rev. D **47**, 3021 (1993).
[9] M. Baker, J. Ball and F. Zachariasen, Phys. Rev. D **51**, 1968 (1995).
[10] S. Jacobs, M. Olsson and C. Suchyta, Phys. Rev. D **33**, 3338 (1986).
[11] L. Fulcher, in *Proceedings of the International Conference on Quark Confinement and the Hadron Spectrum*, 1994, edited by N. Brambilla and G. Prosperi (World Scientific, Singapore).
[12] L. Fulcher, to be published in *Proceedings of the International Conference on Quark Confinement and the Hadron Spectrum*, 1996, edited by N. Brambilla and G. Prosperi (World Scientific, Singapore).
[13] A. Barchielli, N. Brambilla, and G. Prosperi, Nuovo Cimento **103**, 59 (1990).
[14] H. Crater and P. Alstine, Phys. Rev. D **46**, 766 (1992).
[15] H. Crater and P. Alstine, Foundations of Physics **24**, 297 (1994).
[16] J. Ball in *Proceedings of the International Conference on Quark Confinement and the Hadron Spectrum*, 1994, edited by N. Brambilla and G. Prosperi (World Scientific, Singapore).
[17] G. Hardekopf and J. Sucher, Phys. Rev. A **30**, 703 (1984).
[18] L. Fulcher, Z. Chen and K. Yeong, Phys. Rev. D **47**, 4122 (1993).
[19] L. Fulcher, Phys. Rev. D **50**, 447 (1994).
[20] G. Bali, K. Schilling and A. Wachter, to be published in *Proceedings of the International Conference on Quark Confinement and the Hadron Spectrum*, 1996, edited by N. Brambilla and G. Prosperi (World Scientific, Singapore), available as hep-ph/9611226.
[21] G. Bali, K. Schilling and A. Wachter, Southampton preprint (SHEP 96/28), available as hep-lat/9703019.
[22] Because of the model incorporates non-Abelian gauge invariance, this particular choice of gauge should not affect the generality of the results. M. Baker, private communication.
[23] J. D. Jackson, *Classical Electrodynamics* (Wiley, New York, 1975).
[24] Unfortunately, the energies of the singlet S states of the upsilon system have not been measured. Thus, we require theoretical input to determine the hyperfine splitting. We used two calculations that examined running coupling constant effects with care: L. Fulcher, Phys. Rev. D **44**, 2079 (1991) and S. Gupta, W. Repko and C. Suchyta, Phys. Rev. D **39**, 974 (1991). Both obtained very similar results.
[25] W. Lucha, F. Schoeberl and D. Gromes, Phys. Rep. C **200**, 127 (1991).
[26] B. Keister and W. Polyzou, to be published in the Journal of Computational Physics.
[27] D. Gromes, Nucl. Phys. B **131**, 80 (1977).
[28] L. Nickisch, L. Durand and B. Durand, Phys. Rev. D **30**, 660 (1984).
[29] Particle Data Group. R. Barrnett, *et al.*, Phys. Rev. D **54**, 1 (1996).
[30] K. Maung, D. Kahana, and J. Norbury, Phys. Rev. D **47**, 1182 (1993).
[31] D. Stanley and D. Robson, Phys. Rev. D **21**, 3180 (1980).
[32] S. Godfrey and N. Isgur, Phys. Rev. D **32**, 189 (1985).
[33] N. Brambilla and A. Vairo, Phys. Rev. D **55**, 3974 (1997).

FIG. 1. Masses for 1S B mesons as a function of the light quark constituent mass.

FIG. 2. Masses for 1S D mesons as a function of the light quark constituent mass.

FIG. 3. Masses for 1P D mesons as a function of the light quark constituent mass.

FIG. 4. Comparison of the lattice results for V_c with those based on two different forms of V_L used in our calculations.

TABLE I. Matrix elements of the residual potential function $f(r)$ and S-state energy eigenvalues for the upsilon system. The parameters used for this calculation are those listed in Eq. (16) and $\beta = 2.0$ GeV.

Matrix elements	5×5	10×10	20×20	30×30	40×40[a]	Analytic results
$(f)_{00}$	0.38648	0.38648	0.38648	0.38648	0.38648	0.38648
$(f)_{01}$	0.03346	0.03346	0.03346	0.03346	0.03346	0.03346
$(f)_{02}$	0.00318	0.00318	0.00318	0.00318	0.00318	0.00318
$(f)_{03}$	0.00031	0.00031	0.00031	0.00031	0.00031	
$(f)_{11}$	0.35304	0.35304	0.35304	0.35304	0.35304	0.35304
$(f)_{12}$	0.04799	0.04799	0.04799	0.04799	0.04799	0.04799
$(f)_{33}$	0.30244	0.30264	0.30264	0.30264	0.30264	
$(f)_{44}$	0.26930	0.28336	0.28336	0.28336	0.28336	
$E(1S)$	9.47430	9.47368	9.47344	9.47340	9.47341	
$E(2S)$	10.00877	10.00718	10.00703	10.00704	10.00701	
$E(3S)$	10.38178	10.36697	10.36683	10.36683	10.36682	

[a]The Hamiltonian matrix used for the eigenvalues in the last two columns was 20×20.

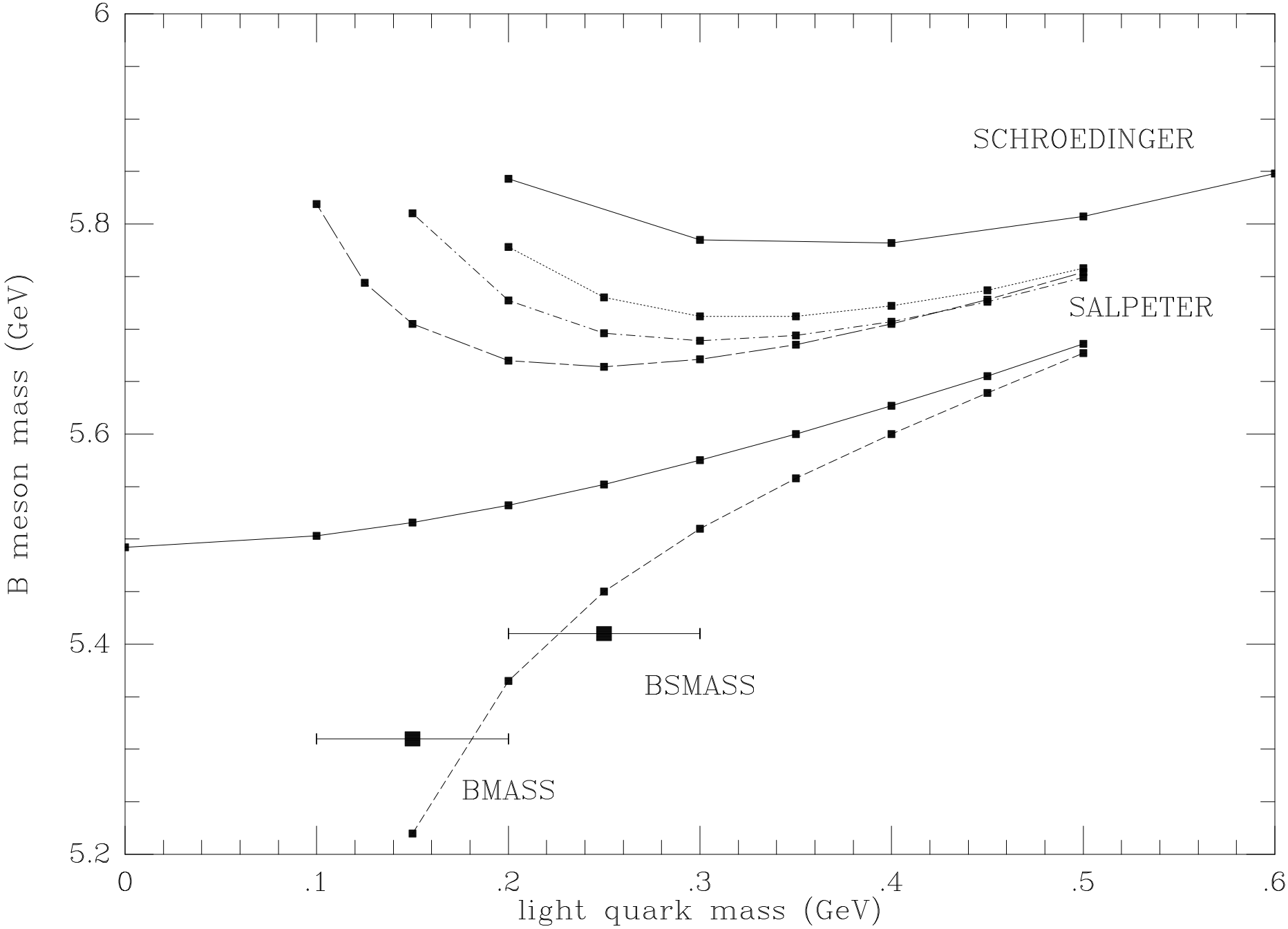
6
5.8
5.6
5.4
5.2
B meson mass (GeV)
0
.1
.2
.3
.4
.5
.6
light quark mass (GeV)
SCHROEDINGER
SALPETER
BSMASS
BMASS

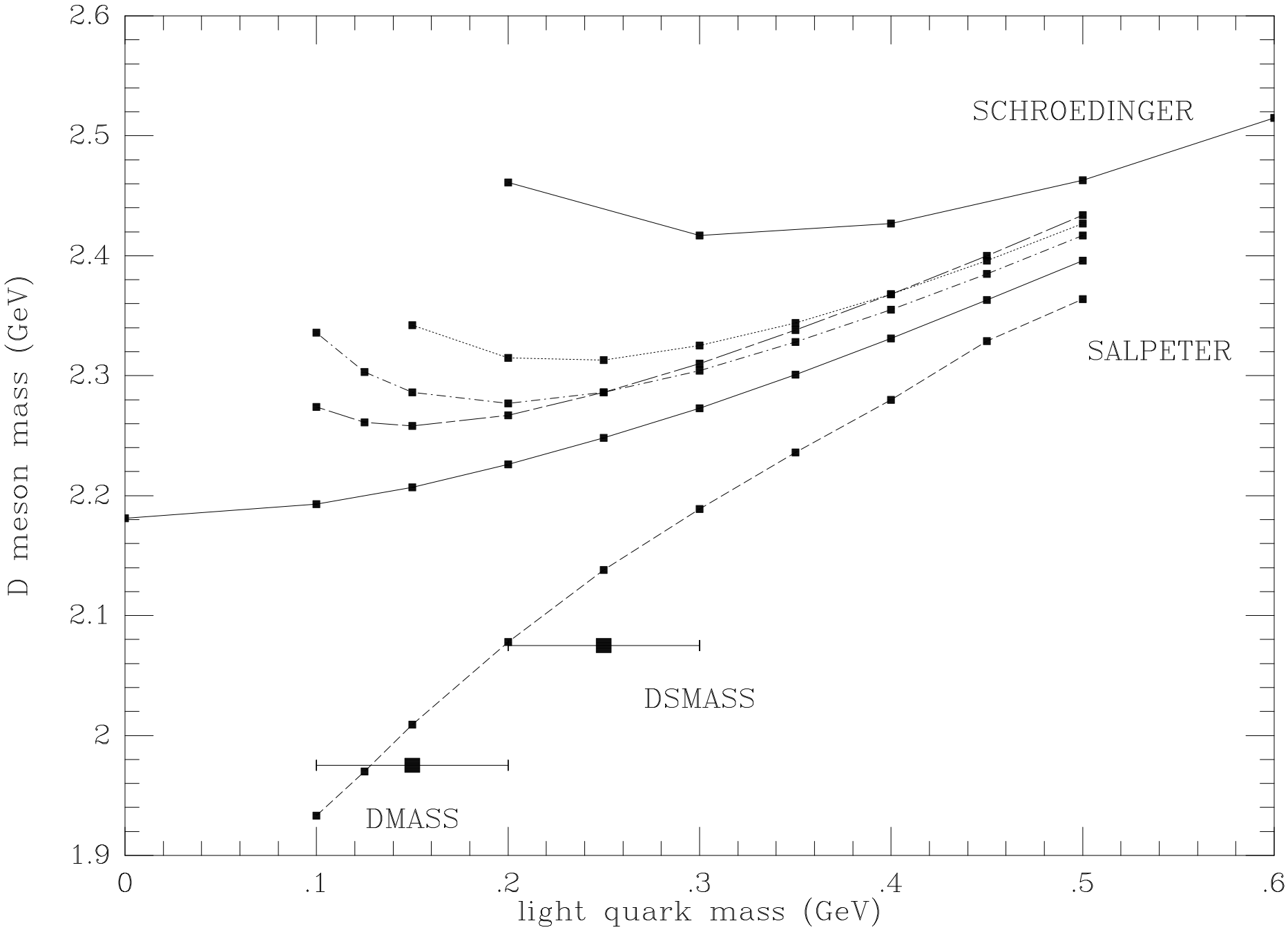
2.6
2.5
2.4
2.3
2.2
2.1
2
1.9
D meson mass (GeV)
0
.1
.2
.3
.4
.5
.6
light quark mass (GeV)
SCHROEDINGER
SALPETER
DSMASS
DMASS

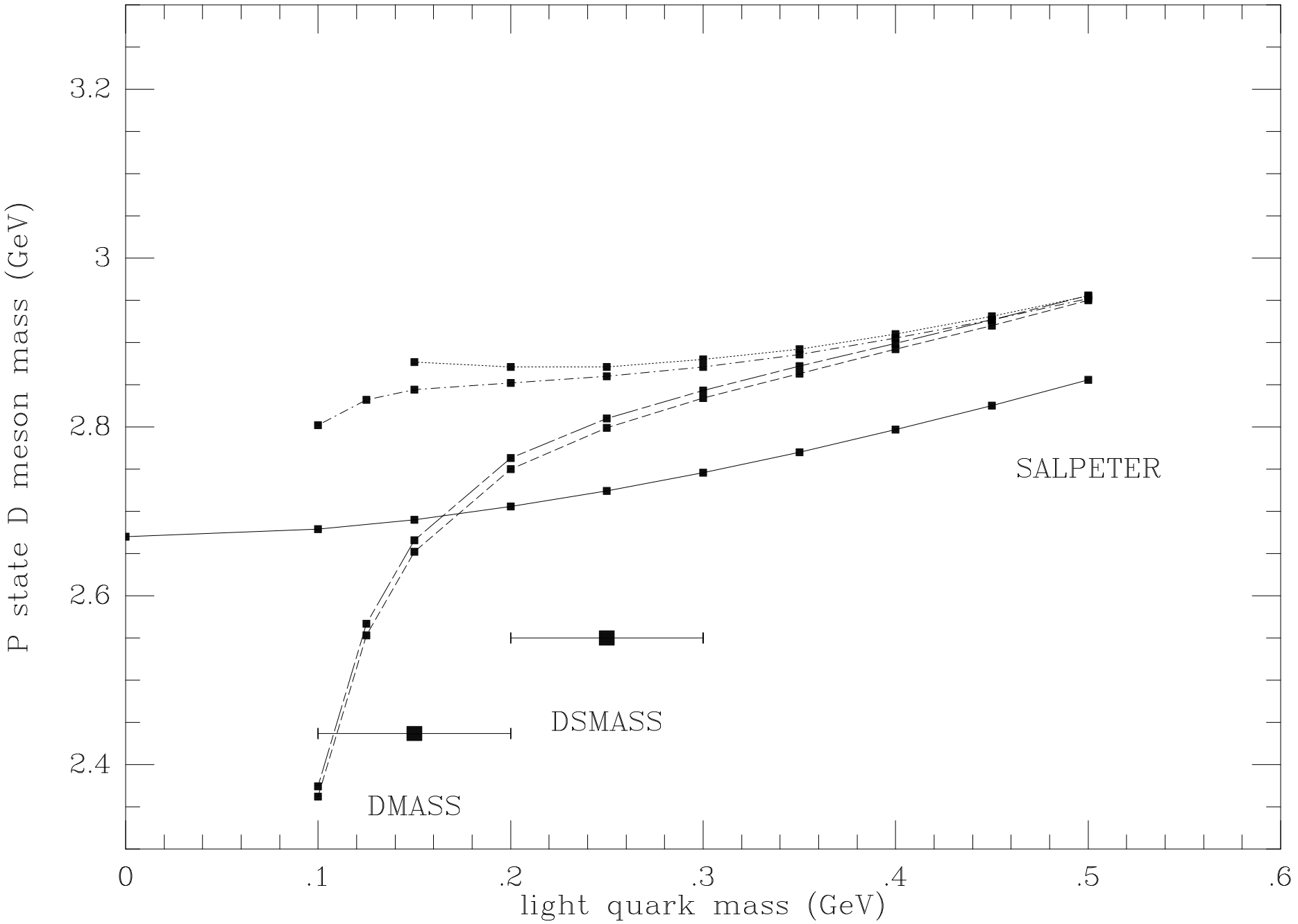
P state D meson mass (GeV)
3.2
3
2.8
2.6
2.4
0
.1
.2
.3
.4
.5
.6
light quark mass (GeV)
SALPETER
DSMASS
DMASS

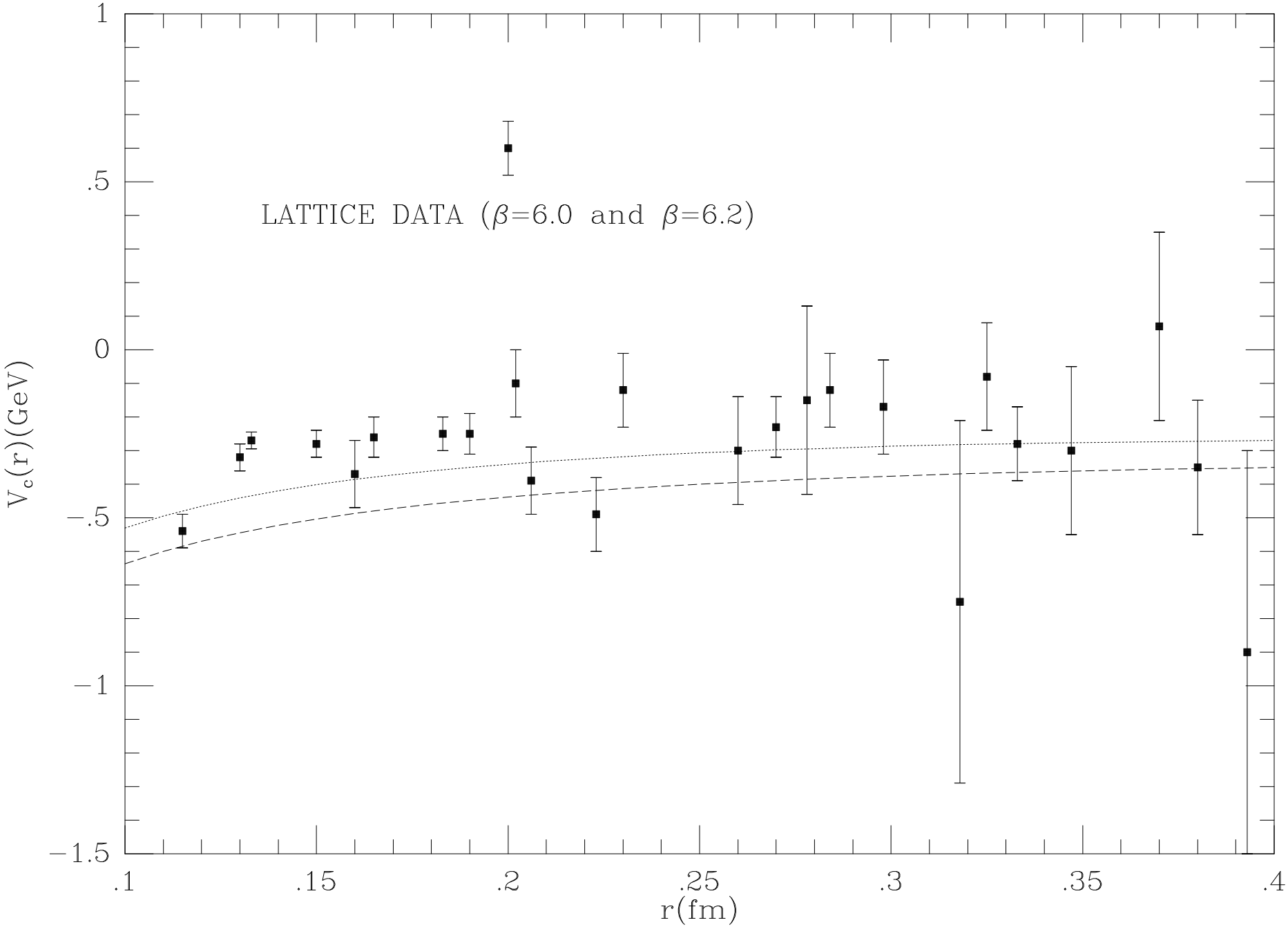
LATTICE DATA (β=6.0 and β=6.2)
$V_c(r)$(GeV)
r(fm)
1
.5
0
−.5
−1
−1.5
.1
.15
.2
.25
.3
.35
.4